Coherent Modes of Global SST and Summer Rainfall over China: An assessment of the regional impacts of the 1997-98 El Niño/La Niña

by

K.-M. Lau and Hengyi Weng[1]

Climate and Radiation Branch, NASA/GSFC, Greenbelt, MD

December 3, 1999

To be Submitted to *Journal of Climate*

[1] SAIC/General Sciences Co., Beltsville, MD

Abstract

In this paper, we have identified three principal modes of summertime rainfall variability over China and global sea surface temperature (SST) for the period 1955-1998. Using these modes, we have assessed the impact of the El Niño/La Niña on major drought and flood occurrence over China during 1997-1998. The first mode can be identified with the growth phase of El Niño superimposed on a linear warming trend since the mid-1950s. This mode strongly influences rainfall over northern China. The second mode comprises of a quasi-biennial tendency manifested in alternate wet and dry years over the Yangtze River Valley (YRV) of central China. The third mode is dominated by a quasi-decadal oscillation in eastern China between the Yangtze River and the Yellow River.

Using a mode-by-mode reconstruction, we evaluate the impacts of the various principal modes on the 1997 and 1998 observed rainfall anomaly. We find that the severe drought in northern China, and to a lesser degree the flood in southern China, in 1997 is likely a result of the influence of anomalous SST forcing during the growth phase of the El Niño. In addition, rainfall in southern China may be influenced by the decadal or long-term SST variability. The severe flood over the Yangtze River Valley in 1998 is associated with the biennial tendency of basin scale SST during the transition from El Niño to La Niña in 1997-98. Additionally, the observed prolonged drought over northern China and increasing flooding over the YRV since the 1950s may be associated with a long-term warming trend in the tropical Indian and western Pacific ocean. During 1997, the El Niño SST exacerbated the drought situation over northern China. In 1998, the drought appeared to get temporary relief from the La Niña anomalous SST forcing.

1. Introduction

One of the most important natural disasters affecting East Asia is the occurrence of severe flood and/or drought during the summer monsoon season from June through August. During the summer of 1997, southern China (south of the Yangtze River) experienced severe flood, while northern China was gripped by one of the driest season on record. In the summer of 1998, rainfall over some regions of the Yangtze River Valley (YRV) and northeast China almost doubled their normal amounts, causing the most widespread and devastating flood of the century in the country. The flood over the YRV afflicted over 240 million people (about the size of the population of the entire United States), damaged more than 30 millions acres of farmland, and ruined over 11 million acres of crops. In all, the flooding over the YRV and northeast China caused over 3700 human lives and inflicted huge economic loss totaling over 12 billion US dollars (National Climate Center 1998).

Thanks to the worldwide attention on the 1997-98 El Niño/La Niña, it is easy to blame the occurrence of the aforementioned disasters on El Niño/La Niña. An important question, which has both scientific and economic implications, is how much of the disaster can be attributed to El Niño? A related fundamental question is how the effect of El Niño on regional climate variability can be quantified? In a recent study, Lau and Wu (1999) estimated that over the Asian-Australia region as a whole, not more than 50% of rainfall variability can be explained by SST processes. They also pointed out that for regional domains, the estimate could vary substantially. Indeed, numerous past studies have showed that there are no consistent relationship between El Niño and rainfall over China as a whole (Ropelewski and Halpert 1988). As a result, schematic rainfall map in the NOAA NCEP homepage on El Niño impacts depicts a large void in the region of East Asia, in contrast to a distinctive negative anomaly center over the India subcontinent (http://iri.ucsd.edu/hot-nino/impacts/india).

A number of recent studies have pointed out the need to subdivide the rainfall variability over China according to its natural regimes and/or fundamental time scales. For example, Wang and Zhao (1978), Huang and Dai (1984), Miao and Lau (1990) and

Shen and Lau (1995) identified a pronounced quasi-biennial (QB) signal in rainfall variability over a broad region in the vicinity of the YRV and sea surface temperature (SST) variability in the Indo-Pacific basin. The QB signal was also found to modulated by longer timescales, i.e., decadal-interdecadal, variation (Nitta and Hu 1996; Chang et al. 1999). Wang and Shi (1992) found different impacts of two kinds of ENSO (El Niño-Southern Oscillation) events on the summer rainfall in China, depending on whether the event first appeared in spring or fall. They also indicated that not all severe droughts or floods over China were associated with El Niño/La Niña events. Ni et al. (1997) studied the correlation between Nino-3 index and a reconstructed rainfall field based on the first four EOF (empirical orthogonal function) modes. They found that only about 30% of rainfall anomaly, especially that in the middle and lower reaches of Yangtze River and southern China, was related to ENSO. More recently, Weng et al (1999, hereafter referred to WLX) identified dominant modes of rainfall patterns that were related to global SST. They showed that the rainfall variability of the YRV is correlated with a dipole SST anomaly in the western subtropical Pacific and that regional summer rainfall variability over China was the result of interplay of various interannual to interdecadal modes. In this paper, we expand on the analysis of WLX, with an emphasis on using coherent modes of rainfall and SST to assess the possible influence of global SST variability on the flood and drought occurrences over China in 1997-98.

Section 2 briefly describes the data and the methodology used. Section 3 reviews historical rainfall distribution and observed rainfall and SST anomalies during 1997 and 1998 summers. Section 4 describes the dominant modes of co-variability between China rainfall and global SST, including a discussion of the physical interpretation of the dominant modes, as well as the dominant timescales contained in these dominant modes. Section 5 unravels the 1997-98 rainfall and SST anomalies based on a mode-by-mode synthesis of the rainfall anomalies. Section 6 presents the main conclusions of the paper.

2. Data and analysis methodology

The China rainfall used in this work is based on a 160-station monthly rainfall total for the period 1951-98, courtesy of Prof. S.-W. Wang, Beijing University, China. The

stations have been chosen to maximize spatial uniform data coverage and continuity (see Fig. 1a). Note that the stations are relatively uniform with good coverage over the eastern portion of the continent, and to a lesser degree over the northeastern portion. Over the desert and semi-arid regions of northwestern China, where the JJA rainfall total is less than 50mm (Fig. 1b), the spatial coverage is quite poor, especially the southwestern region. The spatial variability is therefore highly uncertain over these regions. Our analysis, however, will be more weighted towards the heavy precipitation region of southern and eastern China, where the JJA rainfall total may exceed 500mm (Fig. 1b). The SST data covers the period of 1955-98, with monthly and 10°x10° lon-lat resolution, provided by the National Oceanic and Atmospheric Administration (NOAA, Barneston 1994). The anomalies are defined as deviations from climatologies over the above periods. As in WLX, we used Singular Value Decomposition (SVD) to identify dominant modes of rainfall-SST covariability (Bretherton et al. 1992; Wallace et al. 1992). For time scale analysis, we used the Morlet wavelet transform as described in Weng and Lau (1994) and Lau and Weng (1995).

3. Preliminary observations

a) Historical rainfall distribution

The complex nature of the rainfall variability over China in relationship to El Niño is demonstrated in Fig. 2. Here, the distribution of summer rainfall anomalies according to the entire data record (shaded) and according to warm (solid) and cold (dotted) events in the eastern Pacific Ocean are shown for different regions in China. We choose the warm and cold summers similar to those used by Tomita and Yasunari (1993) and Trenberth (1997). The warm events comprise of 12 summers, which are 1953, 57, 65, 69, 72, 77, 82, 83, 86, 87, 92 and 97. We choose the same amount of cold summers, i.e., 1954, 56, 64, 71, 73, 76, 84, 88, 90, 94, 96 and 98. Some "warm" or "cold" summers were chosen in a year when an El Niño or a La Niña event was just ended (based on Niño3-SST anomaly) in that spring, but its impacts on global and regional climate might still in effect in the following summer. According to our criteria, 1976 and 1996 were counted as cold events while 1977 as warm event. The domain chosen for each regions

are a) all-China, which includes all the 160 stations, b) YRV: 29°-32°N, 105°-122°E, 21 stations, c) southern China: 22°-25°N, 105°-117°E, 11 stations, and d) northern China: 36°-41°N, 105°-12°E, 23 stations. The reasons for the choice of the above domains will become obvious subsequently, when the SVD rainfall modes are discussed.

For all-China rainfall (Fig. 2a), the long-term mean distribution is nearly Gaussian, with zero mean. When stratified into warm and cold events, the rainfall distributions suggest a separation between the warm and cold events favoring overall rainfall reduction for the former and increase for the latter. However, it may also be argued that neither distribution is well separated from the mean distribution. Hence there is only a marginal signal, at best, for all-China rainfall with respect to warm and cold events. Interestingly, the rainfall anomaly over YRV and South China (Figs. 2b and 2c) shows a much wider spread, with almost a white-noise distribution. For these regions, the distributions for the warm and cold events do not yield a clear separation. This suggests that there may be an intrinsic lack of dominant controlling factors for rainfall variability in these regions and that whatever these factors may be they are not well related to warm and cold events. On the other hand, the rainfall variability over northern China shows a much clearer separation between warm and cold events, with the warm events favoring drier and cold events favoring wetter condition. For warm events, the averaged rainfall is approximately 30 mm (31%) below the summer monthly mean (98mm). For cold events, the averaged rainfall is 20 mm (20%) above the mean. The monthly rainfall there may exceed 80% below (above) normal during extreme warm (cold) events, such as the ones during 1997-98. This substantial differences in regional rainfall anomalies with respect to warm and cold events are consistent with the results of WLX, i.e., the only region in China that shows a robust correlation with the SST anomaly in the equatorial eastern Pacific is in the northern part of the country.

It should be pointed out that a lack of a consistent relationship of the rainfall variability over YRV with El Niño (as shown in Fig. 2b) does not preclude the possibility that individual El Niño can exert influence on the YRV rainfall. As pointed out by Lau (1992) and Shen and Lau (1995), a strong monsoon-ENSO relationship is often accompanied by a strong QB signal. In some monsoon regions this is manifested in the

form of an alternation of dry and wet years. Consider the three well-known major flood occurrences in YRV for our data period, 1998, 1973 and 1954. Fig. 3 shows the monthly rainfall variation for two consecutive years in the three cases. The continuous line represents the climatological seasonal cycle. The excessive rainfall in YRV during 1998, 1973 and 1954 are quite obvious, with 1954 having the largest rainfall excess. Notice also that the phases of the excessive rainfall are not quite the same in all three cases. Most interesting is that in the year before the flood, the YRV region tends to be drier than normal, with a few exceptional months, possibly due to intraseasonal variability. For all three cases, a reversal from below to above normal rainfall conditions seems to occur toward October to November of the year before the flood. It is also noted that the three El Niño events during 1997-98, 1972-73 and 1953-54 have a strong QB component, i.e., a well defined cold event followed immediately the peak phase of a warm event. The summers of 1953 and 1972 are during the warm phase of two so-called biennial-ENSO events as classified by Tomita and Yasunari (1993). The 1997 summer would also be in the biennial-ENSO category as shown later by wavelet timescales in Section 4b. Hence, there may be a more subtle relationship between severe drought and flood associated with the QB signal when El Niño impacts are considered.

In this regard, it is worth noting that the strong 1982-83 El Niño was not followed by a pronounced La Niña and that there were no major flood occurrence over the YRV in 1983. Obviously, QB is not the only signal contributing to YRV rainfall variability, and three cases of severe floods can hardly constitute a statistically significant relationship. The main purpose of the above discussion is for illustration only. In the following we will present more detailed analysis and further elaborate on these preliminary observations.

b) *Observed SST and rainfall anomalies during 1997/98 summers*

The summer (Jun-July-august, or JJA) of 1997 chronicled the growing phase of the 1997-98 El Niño, featuring large positive SST anomalies in the equatorial eastern Pacific extending westward into the dateline (Fig. 4a). The eastern Pacific SST anomaly had risen to 3-4°C above normal, boasting the highest SST ever reached in the equatorial

eastern Pacific in the past 44 years. An extensive pool of cold water was found centered at 40°N 170°E in the extratropical North Pacific to the east of Japan. Notice that the entire Indian Ocean was warmer than normal. The Indian Ocean warming, which was just beginning in JJA, continued on through the fall to winter reaching record level in the late 1997 (Webster et al 1999, Yu and Reneicker 1999). Except for a small region near New Guinea, SST in the entire Indo-Pacific basin was above normal. In 1998 summer (Fig. 4b), cold water was established over the Niño-3 area, with negative anomaly in excess of 1.5°C, signaling the emergence of a La Niña. At this time, while remnant of warm water was still present in the extreme eastern tropical Pacific, the cold pool in the North Pacific during 1997 gave way to a warm pool. The latter was the extension of a large body of warm water covering the entire western Pacific and Indian Ocean. Along the equator, the SST began to develop into a seesaw pattern with warm western Pacific/Indian Ocean and cold central/eastern Pacific. A similar seesaw was also found over the subtropical north Pacific with a warm center at 20°N, 150°E and a cold center off the coast of North America near 30° N. Notice that the Indian Ocean remained relatively warm in both years.

The East Asian monsoon was extremely anomalous during 1997 and 1998. In 1997, the anomaly rainfall distribution featured the classic "North-Dry/South-Wet" pattern, with the dividing line near 25°N-30°N (Fig. 4c). This is a well-known anomalous rainfall in China known as *bei-han/nan-lao*. The rainfall pattern was consistent with the following report: *The Yellow River and the Huai River (40°N) regions of northern China was gripped by the most serious drought since 1972. Wild spread flooding were reported in regions in southern and southeastern China. The Guandong province and Hong Kong had rainfall 300-500 mm in excess of the climatological mean.* (National Climate Center 1998).

In the summer 1998, the rainfall pattern changed dramatically. Most areas in China, except for the southeastern coastal region and central northern portion had above normal rainfall. The heavy rainfall was concentrated in the central and southern parts (excluding the southern coastal region) of the country. In the YRV region, especially near the mid- and upper reaches of the Yangtze River, the summer rainfall total exceeded

the normal by 300-500 mm (about doubled). Another area of heavy rainfall was found in northeastern China, where the rainfall total also exceeded the mean by 200 mm (about doubled). The above descriptions show that the rainfall anomalies over China underwent a dramatic shift from 1997 to 1998. This shift occurred at the time when the basin-scale tropical SST was also transitioning from a warm to a cold phase. It is therefore naturally to think that the shift in rainfall and the basin-scale SST evolution may be linked. In the remainder of this paper, we will further elaborate on various possible linkages. First, we will identify and provide physical interpretation of the dominant modes of China rainfall-SST covariability based on the historical data. Then we assess the impacts of SST on 1997-98 rainfall anomalies based on a mode-by-mode synthesis of observed anomalies, and comparison with some other years.

4. Rainfall-SST covariability modes

This section presents results of a SVD analysis on the rainfall and SST field for the period 1955-1998. The analysis for the period 1955-97 was carried out by WLX. The general characteristics of these coupled SVD modes are already described in WLX. In this section, we have carried out additional analyses, aimed at a physical interpretation of the dramatic shift in rainfall and SST during 1997-98. To ensure the robustness of our results, the SVD computations have also been carried out with the years 1997 and 1998 removed. Results (not shown) indicate that the modal patterns are basically unchanged. Hence the SVD modes describe intrinsic modes of covariability between the regional rainfall in China and the global SST, which are not unduly biased by the 1997 and 1998 anomalies.

In the following, we use the suffix *s* and *r* to denote the SST and rainfall SVD modes, respectively. In the temporal domain, each principal component (PC) (or "expansion coefficient") has been normalized by its standard deviation (σ). The corresponding spatial pattern has been multiplied by the PC's standard deviation, so that each SVD spatial loading represents approximately the 1-σ magnitude of the component. For the rainfall patterns, instead of presenting the rainfall eigenvectors, we choose to present the heterogeneous correlation patterns, i.e., the correlation of the

observed rainfall anomalies with each PC*s* (for SST field) of the dominant modes (Wallace et al. 1992). This provides an estimate, at every grid location, of the fractional variance of rainfall (=squared correlation) that can be *explained* by the SST modes.

a) Spatial and temporal patterns

1) SVD1

The first SVD mode explains 34.1% of the squared co-variance between SST and rainfall. The spatial pattern (Fig.5a) suggests an El Niño–like structure, with warm water in the eastern Pacific and the Indian Ocean/Western Pacific. There are two extensive cold pools in the extratropical Pacific in both hemispheres, which intrudes the tropics in the central Pacific.

PC1*s* and PC1*r* (Fig. 5b) are correlated at 0.74, and indicate pronounced interannual variability superimposed on a linear warming trend since 1955, with all years, except 1996, in the 1990's, having positive amplitude. This pattern is similar to that identified by Lau and Weng (1999) as a long-term modulated El Niño mode. Major El Niño events can be identified, but not one-to-one, with the interannual variability of this coupled mode. Some extreme events occurred in non-El Niño years, e.g., 1980, 1969. 1959-1961. Since there is generally a time lag of two seasons between peak monsoon rainfall and SST in the eastern equatorial Pacific, this mode can also be identified with the growing phase of basin-scale warm events (not necessarily identical with El Niño), which are linked to the Asian monsoon.

The heterogeneous rainfall correlation associated with SVD1*s* (Fig. 5c) shows an alternating high-low-high rainfall pattern spanning central, northern and extreme northeastern China. Notice that where the correlation is highest in northern China, the maximum is only about 0.3 (or about 9% of the local rainfall variance). Hence, only a small fraction of the point variance can be explained by the variability associated with this dominant mode. In the semi-arid regions of western China, the correlation is also relatively high. However, as noted earlier, spatial sampling may be a problem here.

2) SVD2

SVD2 explains 15% of the total squared covariance between rainfall and SST. The SVD2*s* pattern (Fig. 6a) is associated with an emerging cold event, and in a number of cases can be identified with a developing La Niña, e.g., 1998, 1988. The SST pattern features a see-saw between the western Pacific and the eastern Pacific, with the dividing line near the dateline at the equator, but tilting eastward with latitude in both hemispheres. The center of the negative anomaly is over the Niño-3 region, while the centers of the positive anomalies are in the waters surrounding the maritime continent and in the subtropical western Pacific. The Indian Ocean SST is above normal, with a weak east-west SST gradient, whose sense is opposite to that in the Pacific. The SST pattern is similar to that associated with the QB mode in the East Asian monsoon region (Shen and Lau 1995).

The correlation between PC2*s* and PC2*r* is at 0.71. The reversal in sign of PC2*s* and PC2*r* between 1997 and 1998 suggests a strong biennial tendency (Fig. 6b). A strong biennial signal (more so in the rainfall PC) can also be discerned in different portion of the time series, e.g., the 1990s and the mid-1970s to the early 1980s. As will be shown later by wavelet analysis, the quasi-biennial timescale is dominant in this mode.

The heterogeneous rainfall pattern associated with this mode (Fig. 6c) shows increased rainfall in a broad swath from southwest to northeast China with the strongest loading (>0.3) over the YRV and the extreme northeastern portion of China. The rainfall and SST pattern resembles those obtained by Shen and Lau (1995), who identified the patterns as the dominant QB mode in East Asia monsoon rainfall and SST variability

3) SVD3

While the fraction of the squared covariance explained by this mode, 10.8%, is not very high, the correlation between PC3*s* and PC3*r* (=0.77) is the highest among the first three SVD modes. This is due to the long time scale inherent in this mode. The SST distribution (Fig. 7a) features a wavelike structure linking the eastern equatorial Pacific, the subtropical eastern and the North Pacific, over the eastern part of the Pacific basin. No clear SST patterns are found over the Indo-western Pacific tropical oceans.

Both PC3*s* and PC3*r* in Fig. 7b show that positive and negative anomalies tend to cluster around decades (see discussion in next section). Superimposed on the decadal variations are an apparent trend, favoring positive anomalies since the 1980s, and negative anomalies in the 1950s and in the early to the mid-1960s. The dominant timescale of this mode and the pronounced features in the SST field in the subtropical eastern North Pacific suggest a possible connection with decadal scale oceanic thermocline adjustment processes (McCreary and Lu 1994; Gu and Philander 1997).

The heterogeneous rainfall distribution (Fig. 7c) indicates opposite wet and dry regions to the south and north of the Yangtze River. The Inner Mongolia region in northern central China has the same variation tendency with the area to the south of the Yangtze River. According to the PC3*r*, the aforementioned long-term drought over northern China since 1980 may be associated with this decadal-coupled mode.

b) Dominant timescales

In this section we present results of a wavelet analysis of the principal components of the dominant modes to reaffirm the time scales mentioned in the previous section. Each PC*s* and PC*r* of the first three modes are decomposed by Morlet wavelet transform. To allow for comparison of the magnitude, we use the original PCs (without normalization by standard deviation). Figs. 8 and 9 show the global wavelet spectra (left panels) and the real wavelet coefficients (right panels) for SST and rainfall, respectively. In the following, we refer to interannual variability (IAV) as timescales between 2-8 years and decadal-to-interdecadal variability (DIV) as those longer than 8 years.

In SVD1, for SST signal (PC1*s*), the global wavelet spectrum (Fig. 8a) and the real wavelet coefficients (Fig. 8b) show that the IAV is dominant, with a peak around 3.7 years. There are two sidebands at 2.2 years (i.e., the QB signal) and 5.6 years respectively. These are fundamental timescales associated with El Niño (Rasmusson et al. 1990; Tomita and Yasunari 1993; Lau and Sheu 1988). There is also a bidecadal signal around 18-20 years, which appears to be gradually intensifying since the 1980s (Fig. 8b). In addition, the IAV also tends to migrate towards longer time scales in the 1990s. The long-term trend noted in the previous discussion is projected as the longest

resolvable timescale of about 50-years and longer. For rainfall (PC1*r*) (Figs. 9a and 9b) the main features are almost identical to those for SST, but the individual peaks are much less well defined. It is clear that this mode is dominated by IAV related to basin-scale SST variations associated with El Niño, with significant modulation by the DIV variability (see also discussion in previous section).

In SVD2, for SST signal (PC2*s*), a dominant peak is found at the QB time scale of about 2.2 years and a secondary peak at about 10 years (Fig.8c and 9c). The QB signal is strongest in the rainfall variability (PC2*r*) (Figs. 9c and 9d). The wavelet coefficient for PC2*r* (Fig. 9d) shows that the QB signal is quite pronounced in the late 1960s to the early 1970s, weak or almost absent in the 1980s, but becomes pronounced again in the 1990s. Similar amplitude modulation can be seen in PC2*s* with weaker signal (Fig. 8d). Such a QB signal modulated by interdecadal variation in the East Asian summer monsoon and the tropical Pacific SSTs was also found by Chang et al. (1999).

The typical El Niño time scales (averaged as 4 years) are not well reflected in this mode. The decadal signal is comparatively stronger in the SST than in the rainfall field. In the time domain, the decadal signal is relatively weaker in the middle of the record, i.e., in the 1970s, in both fields. An analysis of the correlation into frequency bands show that most of the correlation between SST and rainfall come from the QB signal (not shown). The results here reveal strong modulation of the QB signal by decadal variability. Such a close relationship between the QB signal and decadal variability has also been observed in other climate variables (e.g., Barnston and Livezey 1989; Labitzke and van Loon 1992).

In SVD3, for SST signal (PC3*s*), the time scale is dominated by a decadal oscillation, which stands as a single peak (~10 years) in the PC3s wavelet spectrum (Fig. 8e). Here, the IAV appears as transients, i.e., weak or no correlation between SST and rainfall. The decadal oscillation in this mode appears to have stronger amplitude in the 1960s-70s, but becomes weaker in the last two decades. In the rainfall component, PC3*r*, both the decadal and the biennial signal can be seen. The decadal oscillations appear to be quite robust throughout the entire period (Fig. 8f and 9f). The decadal

variability accounts for much of the high correlation (=0.77) between the SST and rainfall variability in this mode.

5. Reconstruction of the 1997 and 1998 anomalies

In this section, we use the dominant modes to assess the possible impacts of the recent El Niño/La Niña events on the 1997 and 1998 rainfall anomalies over China. Using the first 5 SVDs, we reconstructed the SST and rainfall anomalies for the summer of 1997 and 1998 (Fig. 10). We found that after the first four SVD modes, the inclusion of each additional SVD mode provides very little incremental covariance fraction (< 4%) between constructed and observed fields on average in the past 44 years, and especially for 1997 and 1998. From Fig. 10, it is obvious that the reconstructed fields are quite similar to the observed, with almost all the main features well represented, but weaker magnitude than the observed (see Fig. 4). In the reconstructed 1997 SST (Fig. 10a), the basin-scale warmth of the tropical Indo-Pacific and the subtropical SST dipole can now be seen more clearly. In 1998, the subtropical SST dipole can also be seen, with an unusually warm western subtropics and Indian Ocean (Fig. 10b). The north/dry-south/wet (*bei/han-nan/lao*) rainfall pattern in 1997 is very pronounced (Fig. 10c). In 1998, the rainfall pattern has a strong positive center over the middle YRV (Fig. 10d), with widespread above-normal rainfall over most of China. The spatial correlation coefficients between the reconstructed and the observed patterns are 0.92 for SST and 0.82 for rainfall in 1997, and the counterparts in 1998 are 0.83 and 0.77, respectively. The high correlation attests to the notion that there may be dominant SST related mechanisms influencing the 1997 and 1998 rainfall anomalies over China.

Fig. 11 and 12 show the mode-by-mode reconstruction and cumulative anomaly correlation of the observed rainfall anomalies by the first three SVD for 1997 and 1998 respectively. The observed rainfall fields are reproduced here for visual comparison. In 1997, El Niño related influence (SVD1) accounts for about 50% of the anomaly correlation. The addition of the effect due to the QB mode (SVD2) contributes an additional 23% to the cumulative correlation. According to the opposite signs of PC1*r* and PC2*r* (see Figs. 5b and 6b), the QB impact opposes that due to El Niño over the YRV

in 1997. However, the QB mode and the ENSO influence reinforce and accentuate the drought situation over northern China and the flood situation along the southern coast of China. The first two SVD modes combine to explain up to 73% cumulative correlation. Comparison of Figs. 11b and 11d indicates that the major features of the observed rainfall are captured by these two modes. The inclusion of the decadal mode (SVD3) only marginally increases the anomaly correlation. It should be pointed out that even though SVD3 does not contribute much to the anomaly correlation, some of the long-term, decadal-interdecadal variabilities are already contained in the El Niño and the QB modes (see discussion in Section 4*b*).

The spatial correlation between the El Niño mode (SVD1) and the rainfall anomaly field in 1998 is only 0.29. The addition of the QB mode boosts the correlation to 0.67. Visually, it can be seen that major features in the observed anomalies are again captured by the combination of the two modes. The heavy rain center over the YRV and to a lesser degree the northeast are well captured. Notably absent from the reconstruction are the wet conditions over the southwest, suggesting that these features may not be related to the El Niño or the QB SST variability.

The cumulative anomaly correlation is a measure only of the coherence of the *phases* of the reconstructed and observed patterns. However, for estimating the severity of floods and droughts, knowledge of the magnitude is more important. To estimate the mode-by-mode contribution to the *magnitude* of the anomalies, we use the cumulative relative error variance (*CREV*) defined as

$$CREV_J = \sum_{x,y}[OBS - \sum_{j=1}^{J}(PC_j \times SVD_j)]^2 / \sum_{x,y}(OBS)^2,$$

where *OBS* represents observed rainfall anomaly, the summation over j indicates that the reconstruction is based on the first J cumulative modes, and the summation over x, y indicates that the error is estimated at each grid point and summed up over a designated spatial domain. Figure 13 shows the *CREV* for the first five cumulative modes for rainfall in all China, YRV, southern China and northern China for 1997, 1998, and the average for 1955-98. Here the smaller the *CREV*, the better the reconstruction is as an approximation of the observed rainfall magnitude.

For all-China (Fig. 13a), for the long-term average (1955-98), the *CREV* decreases steadily as more and more modes are included in the reconstruction. The average error remains fairly high (~ 60%) even when the 5th mode is included. For 1997 and 1998, the error due to SVD1 is quite large, i.e., 90% for 1998 and 70% for 1997. The largest reduction in error (compared to the long-term mean) appears to come from SVD2. Further error reduction due to inclusion of higher modes is only minimal. These suggest that as a whole, the all-China rainfall is somewhat affected by the El Niño growth mode (SVD1) in 1997, but more so by the QB mode (SVD2) in 1998. As discussed previously, the all-China region encompasses a number of rainfall regimes and is not a very good measure of regional variability.

The regional error patterns are more revealing. Over the YRV (Fig. 13b), it can be seen that in 1997, and especially in 1998, the QB mode (SVD2) is dominant. The combination of these two modes reduces the error variance to less than 20%, substantially less than the long-term mean. In contrast, in southern China (Fig. 13c), SVD2 seems to have an impact in 1997, but not in 1998 (*CREV* $\geq$120%). Here, higher order modes, in particular SVD4 that has a multi-decadal timescale and same polarity of rainfall over most area of China (not shown), may have a strong contribution. In northern China (Fig. 13d), SVD1 has a strong impact in 1997 (*CREV* $\leq$25%), but has not much influence in 1998 (*CREV* $\geq$100%).

The aforementioned results for 1997-98 are consistent with those discussed with regard to Figs. 2 and 3, i.e., northern China has the most impact from El Niño growing phase, the YRV region has a pronounced biennial variability, and southern China has the most diverse variability, including higher order modes.

6. Conclusions

We have identified three dominant modes of summer rainfall-SST covariability over China. Using these modes, we assess the SST impacts on regional rainfall anomalies in China during 1997 and 1998. The most dominant mode can be identified with the growing phase of El Niño, modulated by a trend since the mid-1950s. The corresponding rainfall pattern, in the sense of a positive principal component, features

above normal rainfall in central, northeastern and western China, coupled to a below normal rainfall over northern China. The trend may be related to the long-term drought experienced over northern China since the early 1970's.

The second mode is dominated by the quasi-biennial oscillation accompanied by decadal variation in the tropical ocean-atmosphere, distinguished by a SST sea-saw pattern between the Indo-western Pacific and the eastern Pacific. In its positive phase, the mode can be identified with the growing phase of La Niña (warm Indo-western Pacific and cold eastern Pacific), coupled to excessive rainfall over the middle reaches of the Yangtze River. The third mode is dominated by a quasi-decadal oscillation, which is characterized by wave-like SST pattern linking the equatorial eastern Pacific to the extratropical northern central Pacific along the coast of North America. This mode may be linked to long-term dry (wet) conditions over northern (southern) China.

The rainfall anomalies over China in 1997 and 1998 were strongly impacted by global SST anomalies. In 1997 and 1998, the anomaly correlation between the reconstructed (based on the first two SVD modes) and the observed rainfall is 0.73 and 0.67, respectively. Since the squared correlation is a measure of fractional variance, this means that on the average over all-China, approximately 53% and 45% of the rainfall variance can be attributed to SST anomalies associated with the El Niño and the QB mode. These represent the largest percentages of explained rainfall variance by global scale SST anomaly in the past 44 years. From a mode-by-mode decomposition, we deduce that the drought in northern China and the flood in southern China in 1997 summer are associated with the growing phase of the El Niño. On the other hand, the flooding over the YRV and over northeast China is associated with the quasi-biennial mode SST, distinguished by a well-defined La Niña, which commenced during the summer of 1998, following immediately the demise of the El Niño.

Finally, a prolonged drought over northern China and increased flood tendency over the YRV since the 1950s may be associated with a long-term warming trend in the tropics, in particular the Indian Ocean and the western Pacific region. During 1997, the El Niño SST forcing exacerbated the drought over northern China. In 1998, the drought appeared to get a temporary relief from the La Niña SST forcing.

Overall, it appears that during 1997and 1998 summers, much of the regional rainfall variability in China has been influenced by the well-defined turn-around, i.e., biennial cycle, in SST anomalies from El Niño to La Niña. Summertime rainfall variability over China is only a part of the vast Asian monsoon system. It remains an intriguing possibility that the Asian monsoon may be the source of biennial variability in El Niño. More work on coupling of regional monsoon variability to El Niño is needed to explore this possibility.

Acknowledgment We are thankful to Prof. Shaowu Wang, Prof. Zhenguo Zhao, Mr. Luke He, and Dr. Daoyi Gong for providing rainfall and SST data and related information, to Dr. K. M. Kim for helps in creating some graphics. This work was supported by the Global Modeling and Analysis Program, the Tropical Rainfall Measuring Mission (TRMM) and the Earth Observing System Interdisciplinary Investigation Program of the NASA/Office Mission to Planet Earth.

References

Barnston, A. G., 1994: Linear statistical short-term climate predictive skill in the Northern Hemisphere. *J. Climate,* **7**, 1513-1564.

Barnston, A. G., and R. E. Livezey, 1989: A closer look at the effect of 11-year solar cycle and the quasi-biennial oscillation on northern hemisphere 700mb height and extratropical North American surface temperature. *J. Climate*, **2**, 1295-1313.

Chang, C.-P., Y.-S. Zhang, and T. Li, 1999: Interannual and interdecadal variations of the East Asian summer monsoon and tropical Pacific SSTs. Part 1: Roles of the subtropical ridge. Submitted to *J. Climate.*

Gu, D., and S. G. H. Philander, 1997: Interdecadal climate fluctuations that depend on exchanges between tropics and extratropics. *Science*, **275**, 805-807.

Huang, J. and L. Dai, 1984: An analysis of the power spectrum of the rainfall in Beijing for 256 years. *Weather in North of China*, **5**, Ed. Y.-L. Zhang, Beijing University Press, 108 - 114.

Labitzke, K., and H. van Loon, 1992: Associations between the 11-year solar cycle, the QBO and the atmosphere, Part V, Summer. *J. Climate*, **5**, 240-251.

Lau, K.-M., 1992: East-Asian summer monsoon rainfall variability and climate teleconnection. *J. Meteor. Soc Japan*, **70 (1B)**, 211-242.

Lau, K.-M. and P. J. Sheu, 1988: Annual cycle, quasi-biennial oscillation, and southern oscillation in global precipitation. J. Geophys. Res. (Atm.), 93 (D9), 10975-10988.

Lau, K.-M. and H.-Y. Weng, 1995: Climate signal detection using wavelet transform: How to make a time series sing. *Bull. Amer. Meteor. Soc.*, **76**, 2391-2402.

Lau, K.-M. and H.-Y. Weng, 1999: Interannual, interdecadal and global warming signals in sea surface temperature. *J. Climate,* **12**, 1257-1267.

Lau, K.-M. and H.-Z. Wu, 1999: Assessment of the impacts of the 1997-98 El Niño on the Asian-Australia monsoon. *Geo. Phy. Lett.*, **26**, 1747-1750.

McCreary, J., and P. Lu, 1994: On the interaction between the subtropical and equatorial ocean circulations: the subtropical cell. *J. Phy. Oceanogr.*, **24**, 466-497.

Miao, J. H. and K.-M. Lau, 1990: Interannual variability of East Asian monsoon rainfall. *Quart. J. Appl. Meteor.*, **1**, 377-382.

National Climate Center, 1998: *Severe floods and anomalous climate in China during 1998.* China Meteorological Administration, Meteorology Press, Beijing, pp. 139.

Ni, Y., L. Zou, and Y. Liu, 1997: Diagnostic study of the impact of ENSO on anomalous Asian summer monsoon and precipitation during the rain season in China. In *Climate Variability in China and Climate Impacts Studies.* Eds. Y. Ding, et al. Meteorological Press, Beijing, pp.235-242.

Nitta, T. and Z.-Z. Hu, 1996: Summer climate variability in China and its association with 500hPa height and tropical convection., *J. Meteor. Soc. Japan*, **74**, 425-445.

Rasmusson, E. M., X. Wang, and C. F. Ropeleski, 1990: The biennial component of ENSO variability, *J. Mar, Systems*, **1**, 71 - 96.

Ropelewski, C. F., and M. S. Halpert, 1987: Global and regional precipitation pattern associated with the El Niño Southern Oscillation. *Mon. Wea. Rev.*, **115**, 1606-1626.

Shen, S. and K.-M. Lau, 1995: Biennial oscillation associated with the East Asian summer monsoon and tropical sea surface temperatures. *J. Meteor. Soc. Japan*, **73**, 105 - 124.

Tomita, T., and T. Yasunari, 1993: On the two types of ENSO. *J. Meteor. Soc. Japan*, **71**, 273 - 284.

Trenberth, K. E., 1997: the definition of El Niño. *Bull. Amer. Meteor. Soc.*, **78**, 2771-2778.

Wallace, J. M., C. Smith, and C. S. Bretherton, 1992: Singular value decomposition of wintertime sea surface temperature and 500-mb height anomalies. *J. Climate*, **5**, 561 - 576.

Wang, S.-W. and W. Shi, 1992: Different impacts of two kinds of ENSO events on the summer rainfall in China. In *On the Roles of the Oceans Regulating and Controlling Climate Variability.* Eds. Y. Zhang, et al. Ocean Press, pp. 76-87.

Wang, S.-W. and Z.-C. Zhao, 1978: Climatic change in China and global atmospheric circulation for the last 100 years. Y.-L. Zhang (ed.), *Proceedings of National*

Conference of Climate Change. Central Meteorological Bureau. Chinese Science Press, 117-130.

Webster, P. J., A. M. Moore, J. P. Loschnigg, and R. R. Leben, 1999: Coupled ocean-temperature dynamics in the Indian Ocean during 1997-98. *Nature*, **401**, (6751) 356-360.

Weng, H.-Y., and K.-M. Lau, 1994: Wavelet, period-doubling, and time-frequency localization with application to organization of convection over the tropical western Pacific. *J. Atmos. Sci.*, **51**, 2523-2542.

Weng, H.-Y., K.-M. Lau and Y.-K. Xue, 1999: Multi-scale summer rainfall variability over China and its long-term link to global sea surface temperature variability. *J. Meteor. Soc. Japan,* **77**, 845-857.

Yu, L., and M. Reneicker, 1999: Mechanisms for the Indian Ocean warming during 1997-98 El Niño. *Geophys. Res. Lett.*, **26**, 735-738.

Figure Caption

Figure 1. **(a)** The 160 stations where the rainfall data are used for this analysis, and the three areas where floods and droughts are discussed in the text. (b) Averaged summer rainfall total for the period of 1955-98. The contour interval is 100mm between solid lines (the dashed lines show 50mm-interval). Areas with more than 200mm and 500mm are light and dark shaded, respectively.

Figure 2. Histogram of rainfall anomaly occurrence in summer months (JJA) for a) China, b) YRV (29°-32°N, 105°-122°E), c) southern China (22°-25°N, 105°-117°E), and d) northern China (36°-41°N, 105°-122°E) for the period of 1951-1998. Shaded area is for all summer months; the areas under solid and dashed lines are for selected El Niño and La Niña summers, respectively. The twelve El Niño summers are 1953, 57, 65, 69, 72, 77, 82, 83, 86, 87, 92 and 97. The twelve La Niña summers are 1954, 56, 64, 71, 73, 76, 84, 88, 90, 94, 96 and 98.

Figure 3. 1997 and 1998 monthly total rainfall (bars) and the 1951-98 mean (line) for a) China, b) YRV, c) southern China, and d) northern China. (Unit: 100*mm*)

Figure 4. Summer averaged SST anomaly for a) 1997 and b) 1998, and summer total rainfall anomaly for c) 1997 and d) 1998. The interval for SST is 0.25°C, and the anomaly greater than 2°C is the shaded darkest. Positive (negative) anomalies are dark (light) shaded. The interval for rainfall anomaly is 50mm, and the anomalies greater than 200mm are shaded darkest.

Figure 5. SVD1 mode: a) spatial pattern for SST (SVD1*s*), b) principal components for both SST (PC1*s*) and rainfall (PC1*r*), and c) heterogeneous rainfall pattern (H1). The positive (negative) anomalies in a) and c) are dark (light) shaded. The interval in a) is 0.25°C, while that in c) is 50mm.

Figure 6. Same as Fig. 5, except for SVD2.

Figure 7. Same as Fig. 5, except for SVD3.

Figure 8. Global wavelet spectra (left panels) and the real wavelet coefficients (right panels, interval is 0.5°C) of the first three leading for 1955-98 summers.

Figure 9. Global wavelet spectra (left panels) and the real wavelet coefficients (right panels, interval is 100*mm*) of the first three leading for 1955-98 summers.

Figure 10. Reconstructed summer SST anomaly patterns for a) 1997 and b) 1998, and the reconstructed summer rainfall anomaly patterns for c) 1997 and d) 1998, base don the five leading SVD modes. Positive (negative) anomalies are dark (light) shaded. The interval for SST is 0.25°C, and the anomaly greater than 2°C is the shaded darkest. The interval for rainfall anomaly is 50mm, and the anomalies greater than 200mm are shaded darkest. The values at the lower left corners in the panels are the spatial correlation coefficients between these patterns and the corresponding observed patterns in Fig. 4, while those at the lower right corners are the percentage of the explained SST or rainfall variance by these reconstructed patterns.

Figure 11. The reconstructed rainfall anomaly patterns for 1997 summer based on accumulative SVD modes for up to the first four modes. The interval is 50mm, and the anomalies greater than 200mm are shaded darkest. The values at the lower right corners in the panels are the spatial correlation coefficients between these patterns and the corresponding observed rainfall patterns in Fig. 4c.

Figure 12. Same as Fig. 11, except for 1998.

Figure 13. Cumulative relative error variance (*CREV*) of reconstructed rainfall anomalies compared with the observed anomalies based on the first five cumulative SVD modes for 1997, 1998 and the average of 1955-98 in the areas of a) all China, b) YRV, c) S. China, and d) N. China.

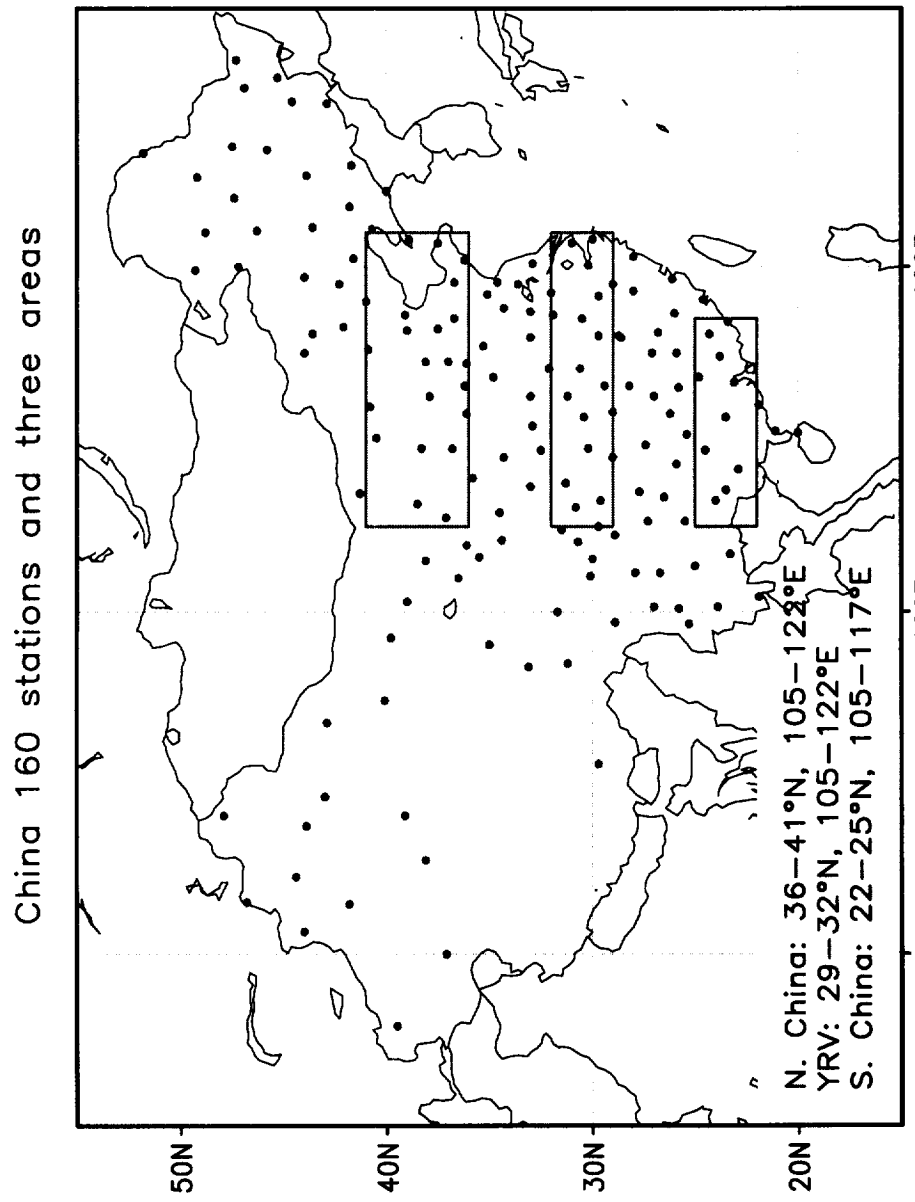
China 160 stations and three areas
50N
40N
30N
20N
80E
100E
120E
N. China: 36–41°N, 105–122°E
YRV: 29–32°N, 105–122°E
S. China: 22–25°N, 105–117°E

Fig.1a

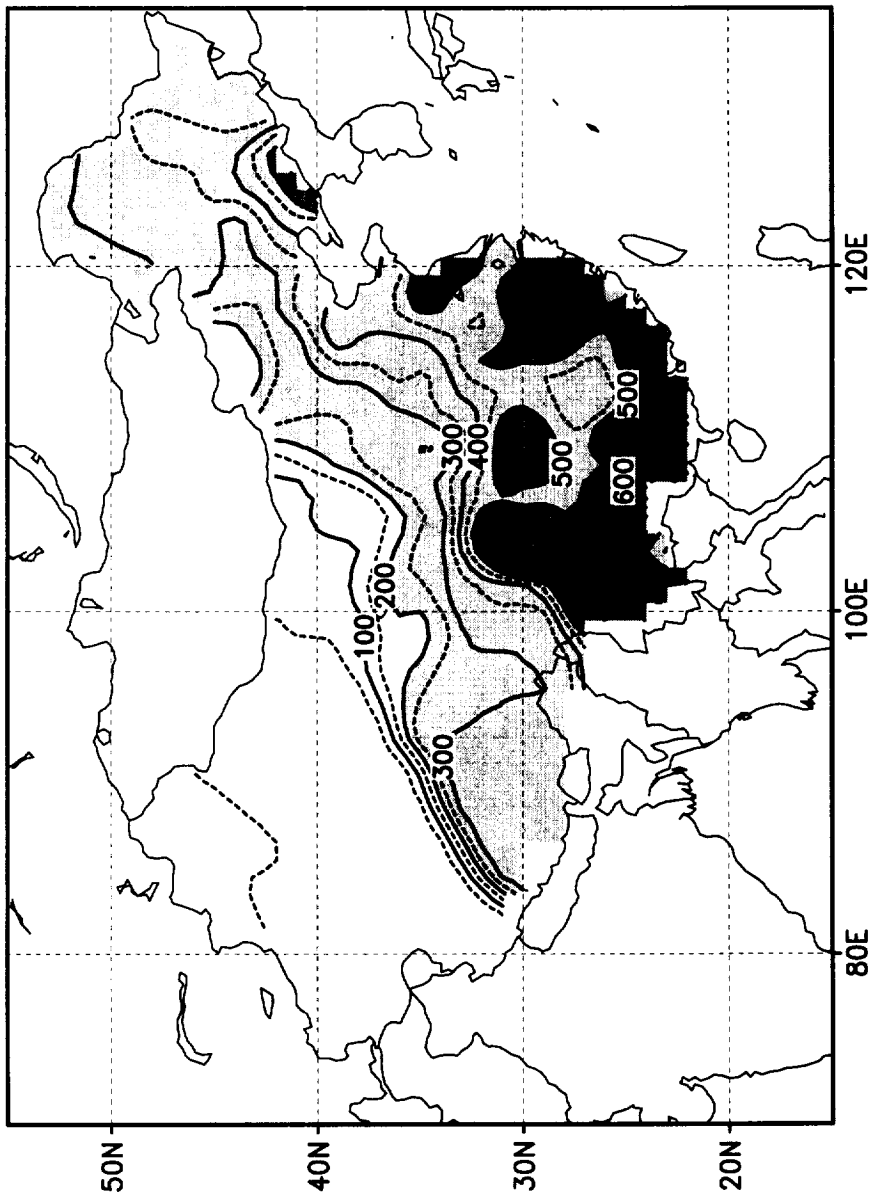

Fig. 1b

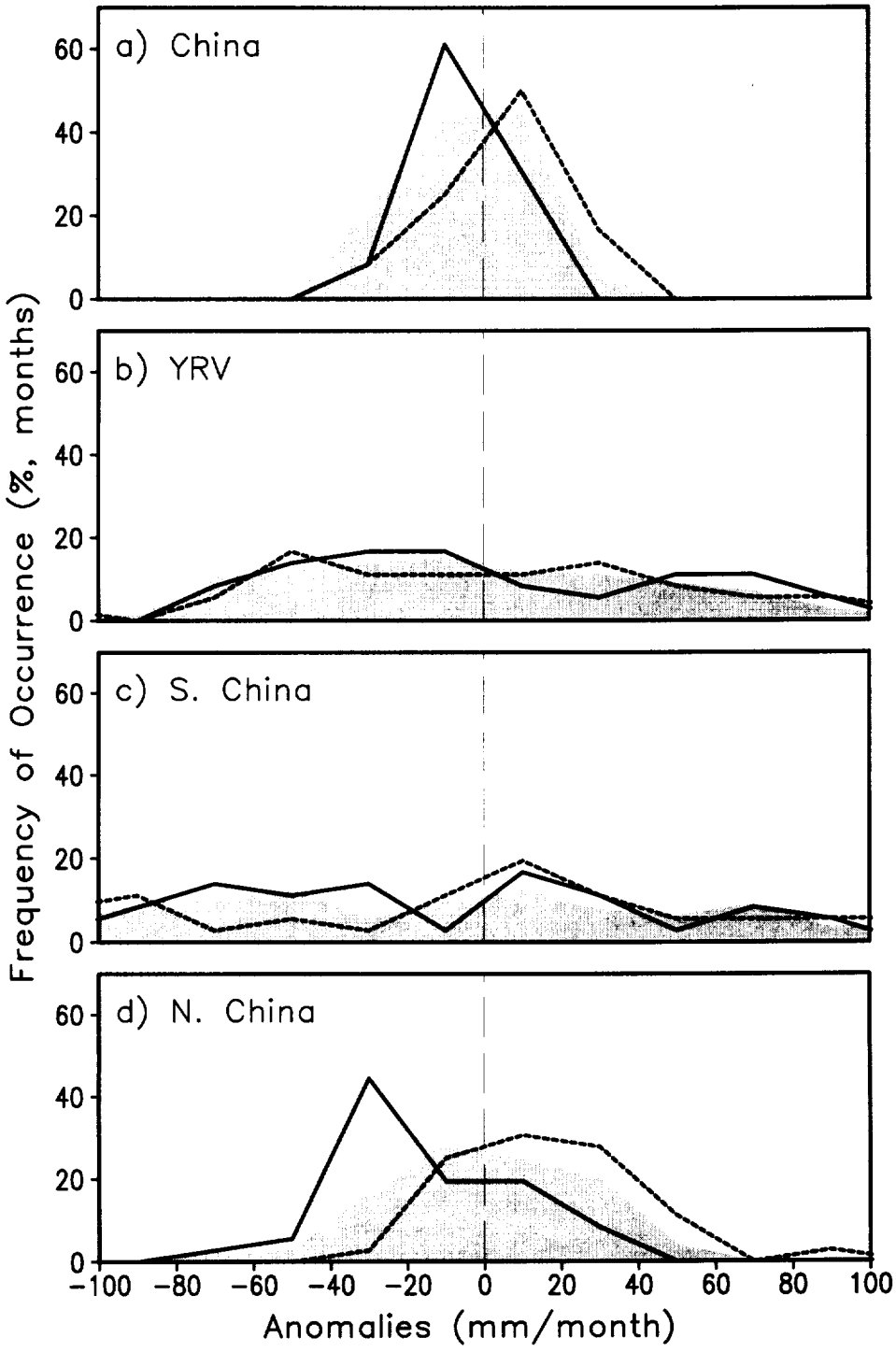
a) China
b) YRV
c) S. China
d) N. China
Frequency of Occurrence (%, months)
Anomalies (mm/month)
0
20
40
60
-100
-80
-60
-40
-20
0
20
40
60
80
100

Fig. 2

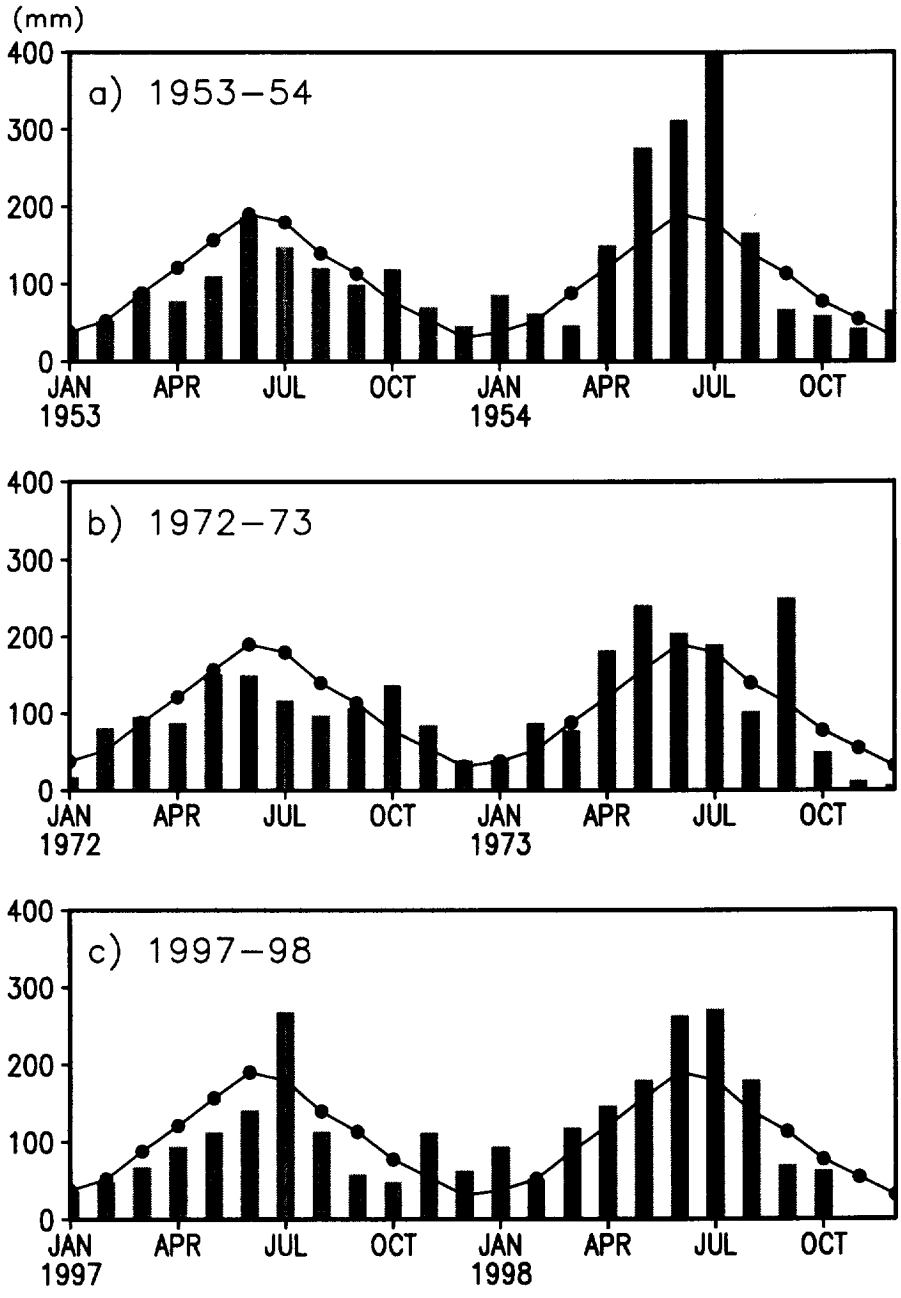
(mm)
400
300
200
100
0
a) 1953–54
JAN 1953
APR
JUL
OCT
JAN 1954
APR
JUL
OCT
b) 1972–73
JAN 1972
JAN 1973
c) 1997–98
JAN 1997
JAN 1998

Fig. 3

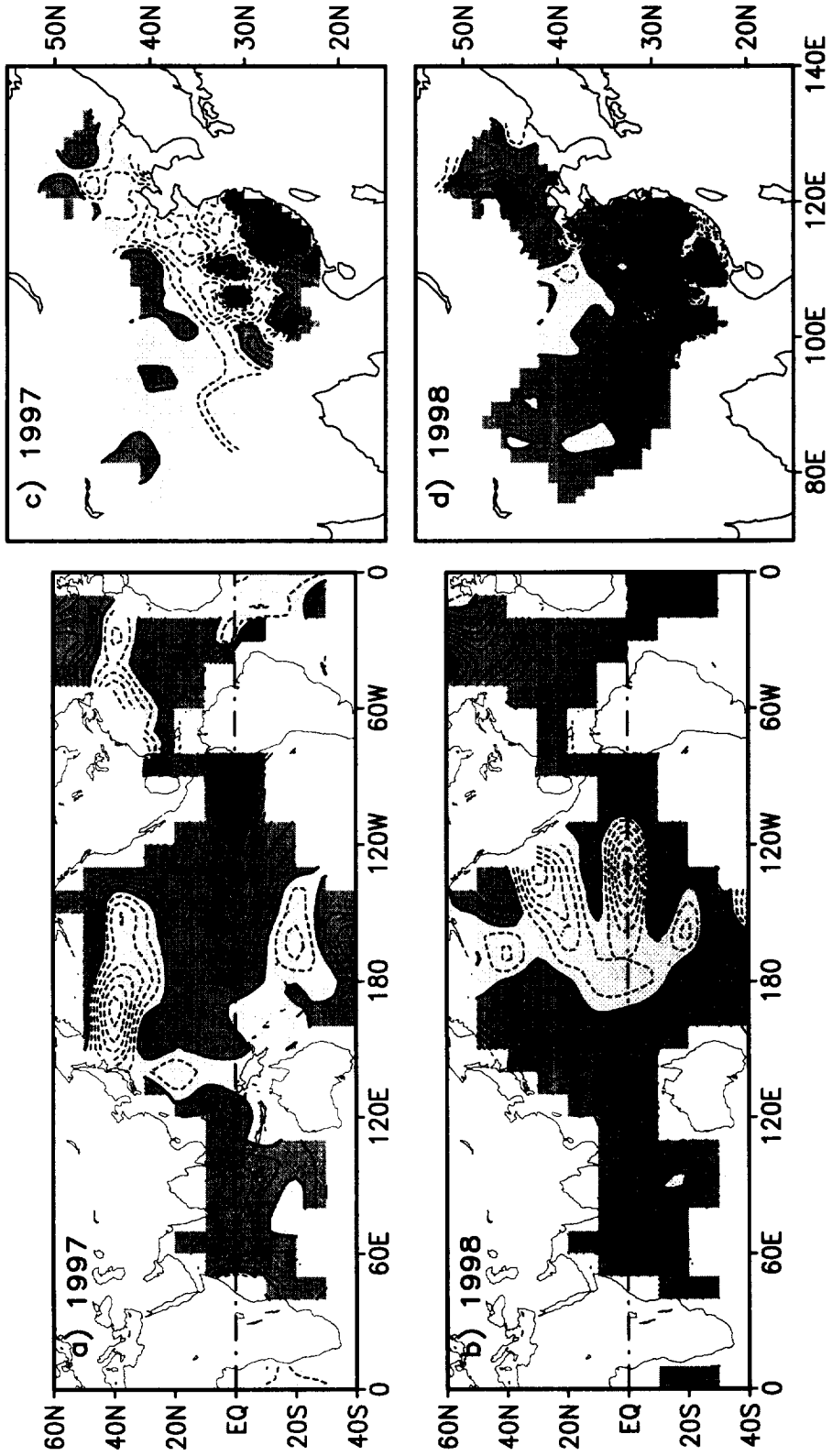
a) 1997
b) 1998
c) 1997
d) 1998
60N
40N
20N
EQ
20S
40S
0
60E
120E
180
120W
60W
50N
30N
80E
100E
120E
140E

Fig. 4

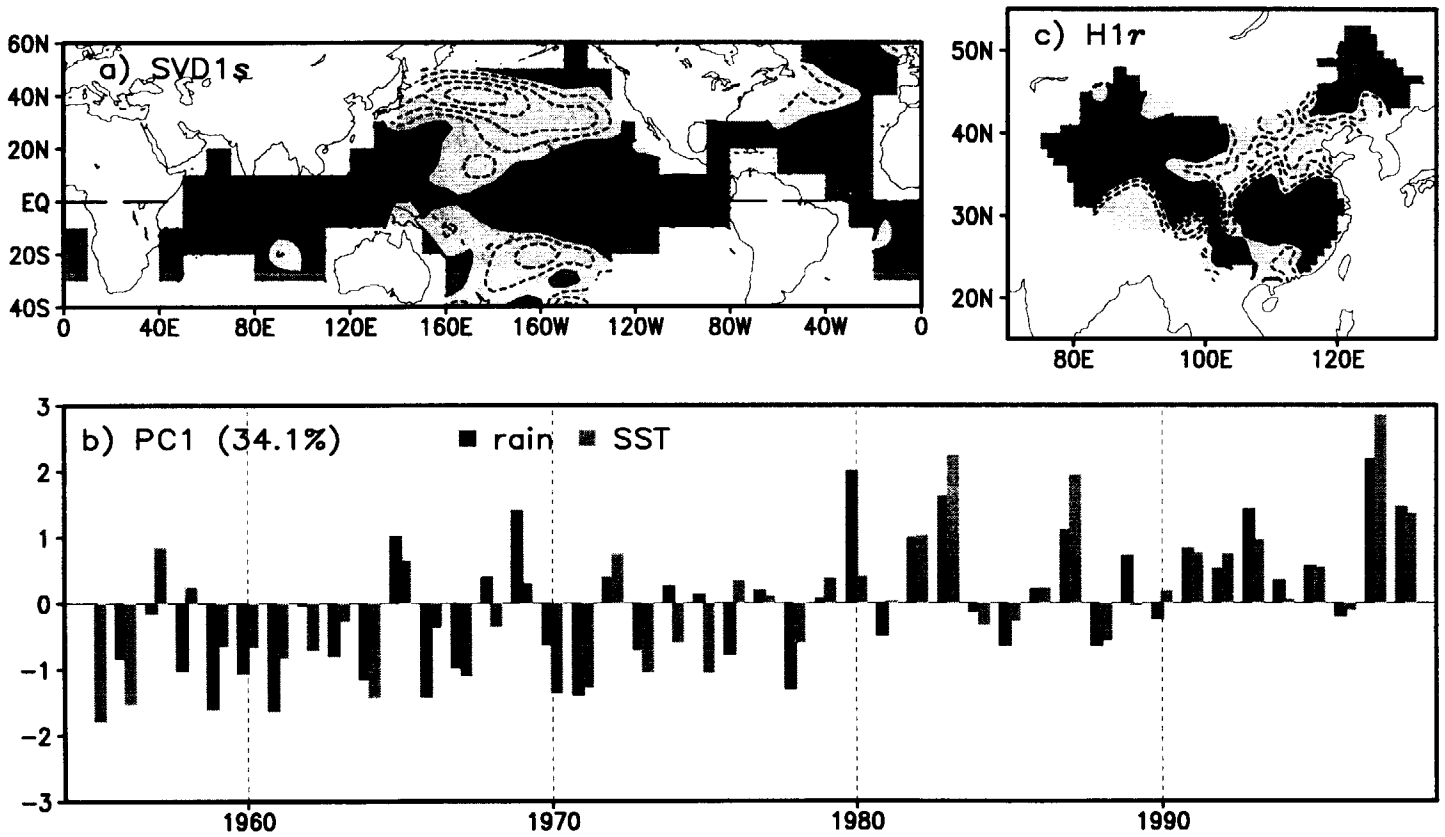
a) SVD1s
60N
40N
20N
EQ
20S
40S
0
40E
80E
120E
160E
160W
120W
80W
40W
0
c) H1r
50N
40N
30N
20N
80E
100E
120E
b) PC1 (34.1%)
rain
SST
3
2
1
0
−1
−2
−3
1960
1970
1980
1990

Fig. 5

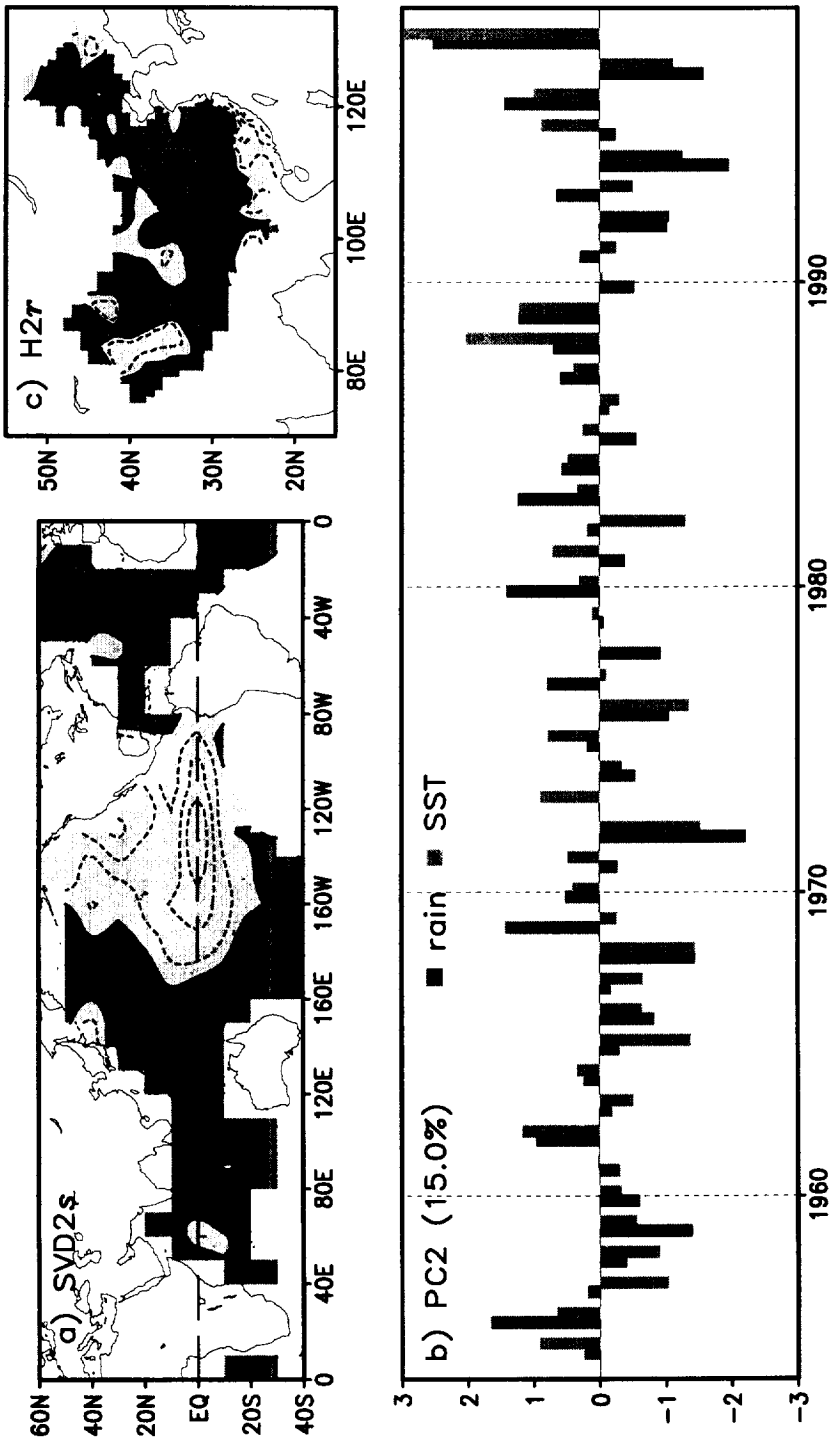
a) SVD2s
60N
40N
20N
EQ
20S
40S
0
40E
80E
120E
160E
160W
120W
80W
40W
0
c) H2r
50N
40N
30N
20N
80E
100E
120E
b) PC2 (15.0%)
rain
SST
3
2
1
0
−1
−2
−3
1960
1970
1980
1990

Fig. 6

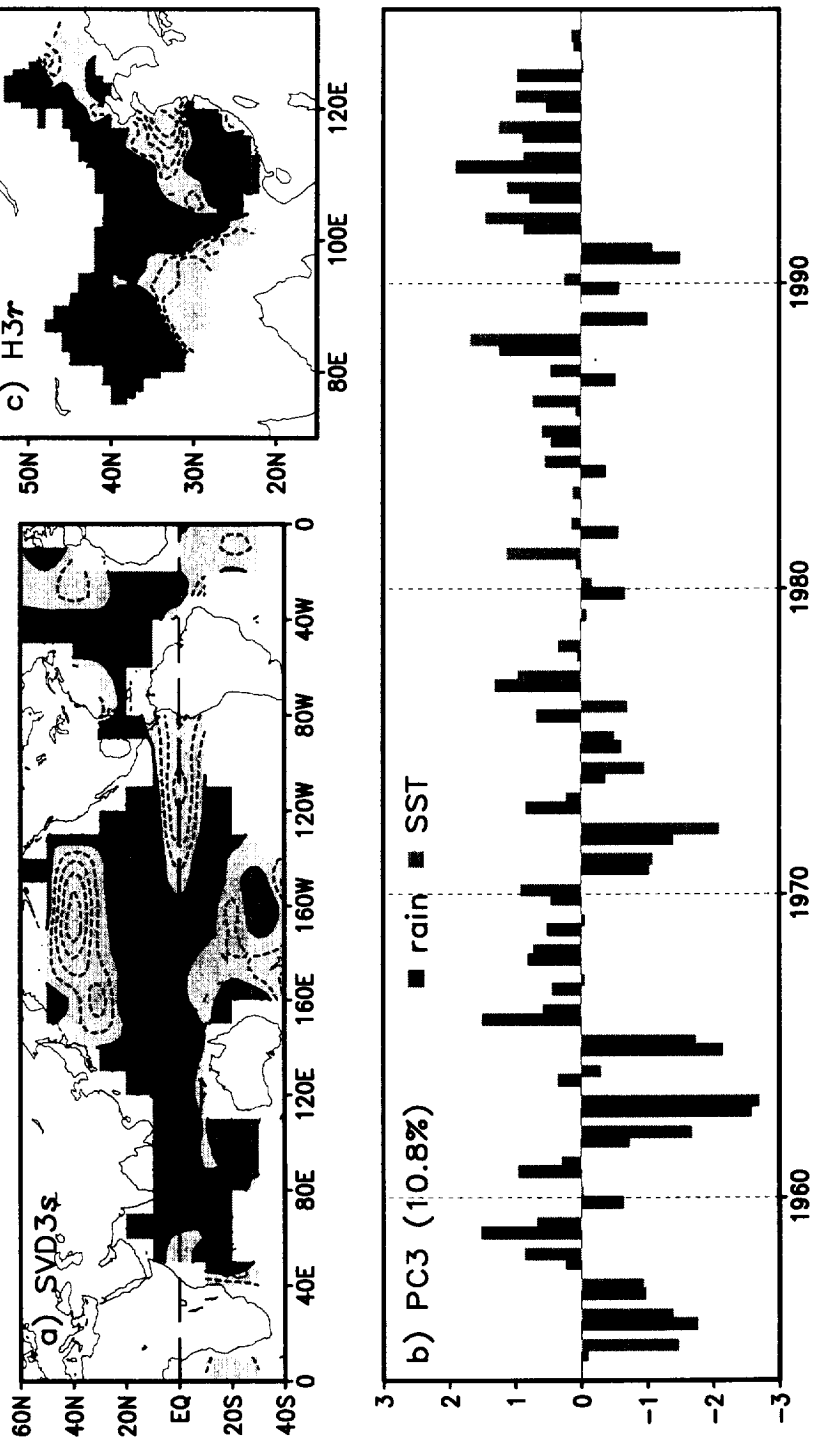
a) SVD3s
60N
40N
20N
EQ
20S
40S
0
40E
80E
120E
160E
160W
120W
80W
40W
0
c) H3r
50N
40N
30N
20N
80E
100E
120E
b) PC3 (10.8%)
rain
SST
3
2
1
0
−1
−2
−3
1960
1970
1980
1990

Fig. 7

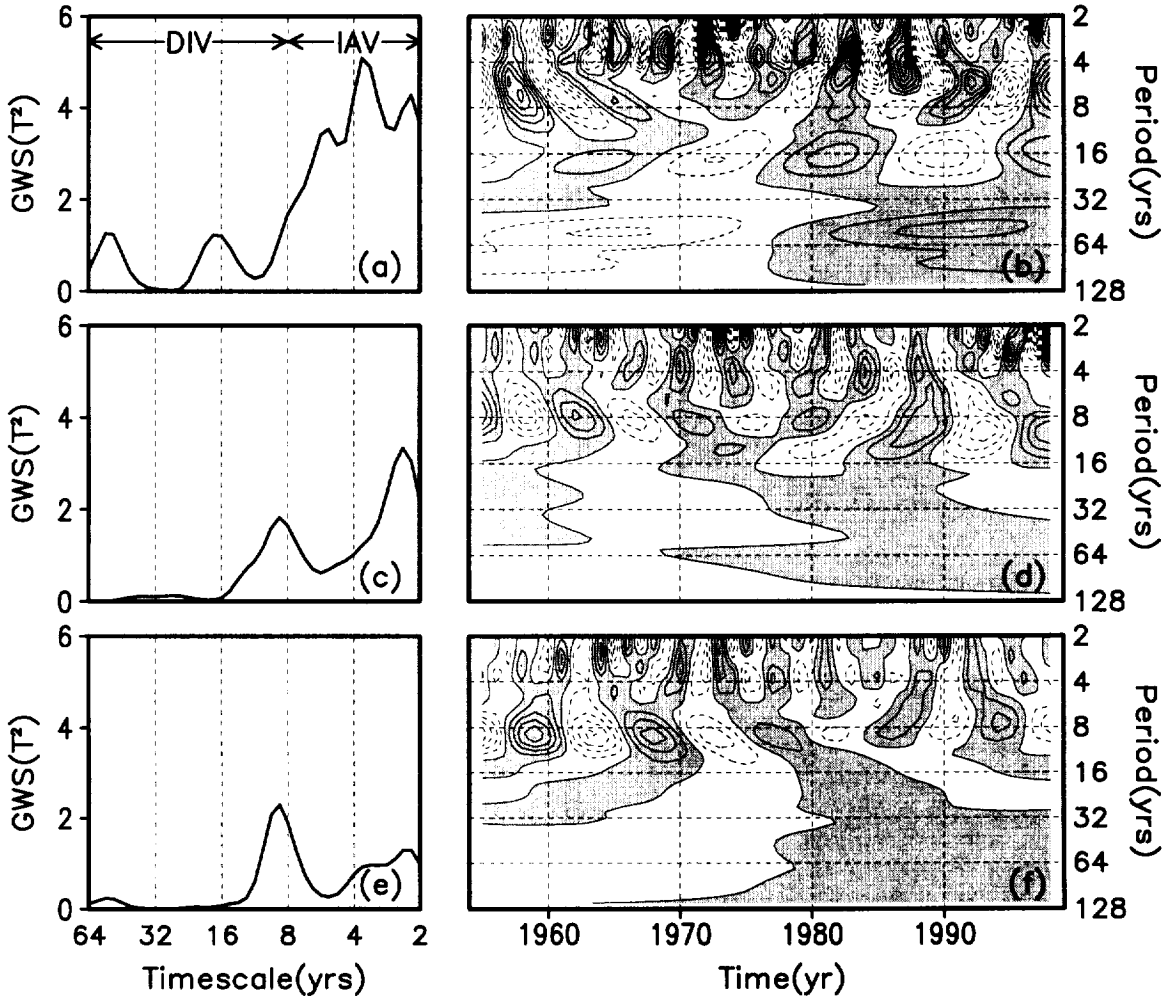
DIV
IAV
GWS(T²)
(a)
(b)
(c)
(d)
(e)
(f)
Period(yrs)
2
4
8
16
32
64
128
0
2
4
6
64 32 16 8 4 2
Timescale(yrs)
1960 1970 1980 1990
Time(yr)

Fig. 8

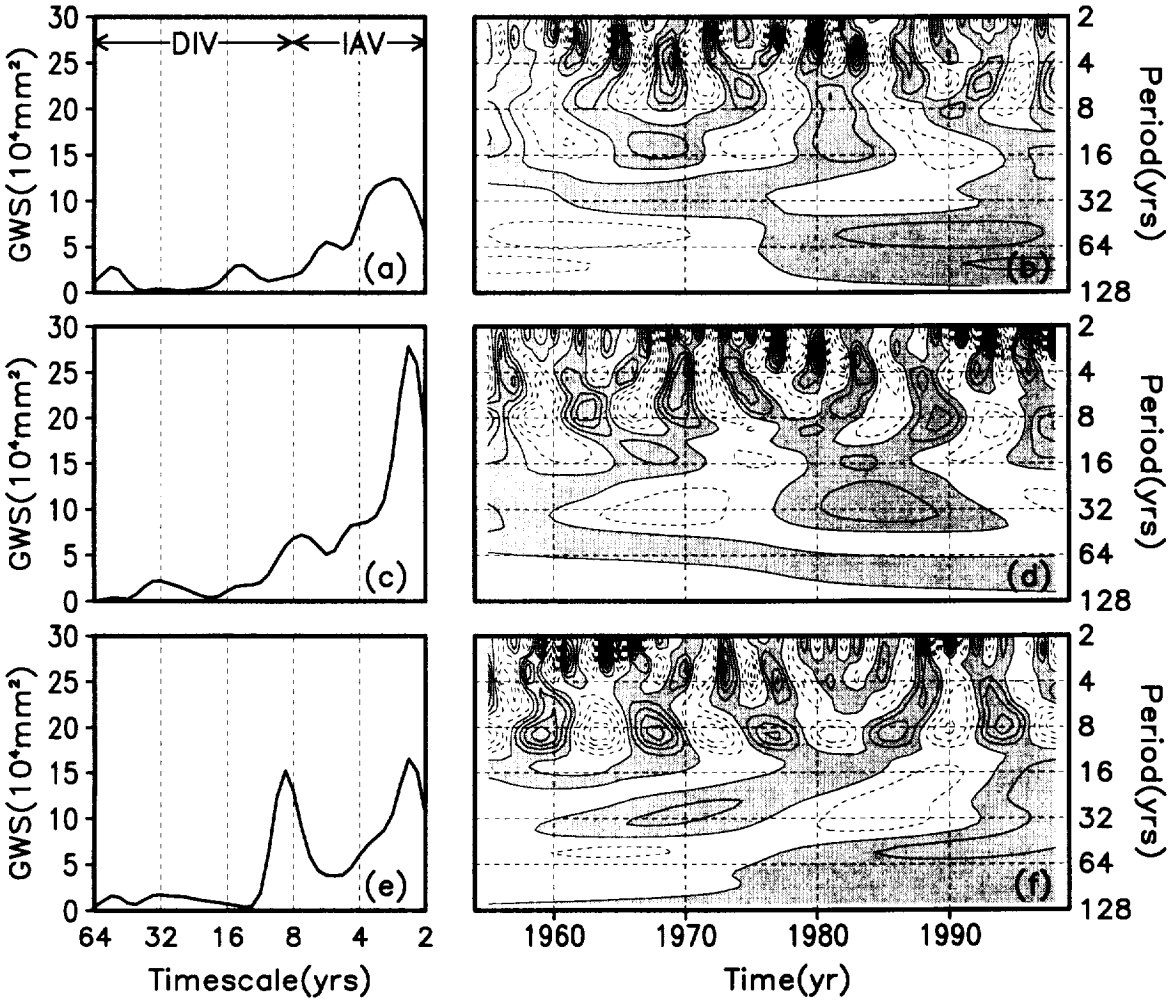
DIV
IAV
GWS(10⁴mm²)
30
25
20
15
10
5
0
(a)
(c)
(e)
64 32 16 8 4 2
Timescale(yrs)
(b)
(d)
(f)
2
4
8
16
32
64
128
Period(yrs)
1960 1970 1980 1990
Time(yr)

Fig. 9

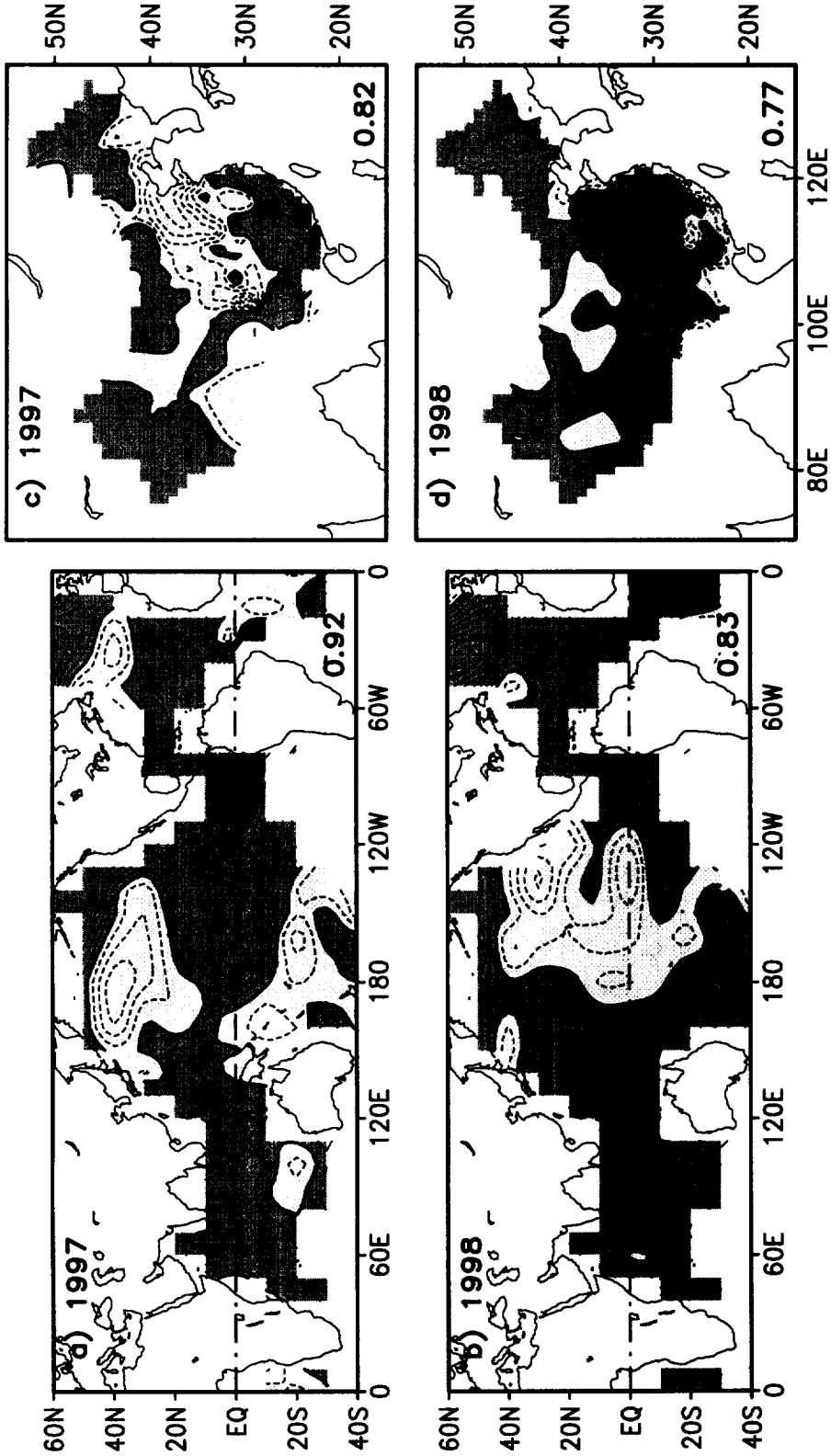
a) 1997
0.92
b) 1998
0.83
c) 1997
0.82
d) 1998
0.77
60N
40N
20N
EQ
20S
40S
0
60E
120E
180
120W
60W
50N
30N
80E
100E
120E

Fig. 10

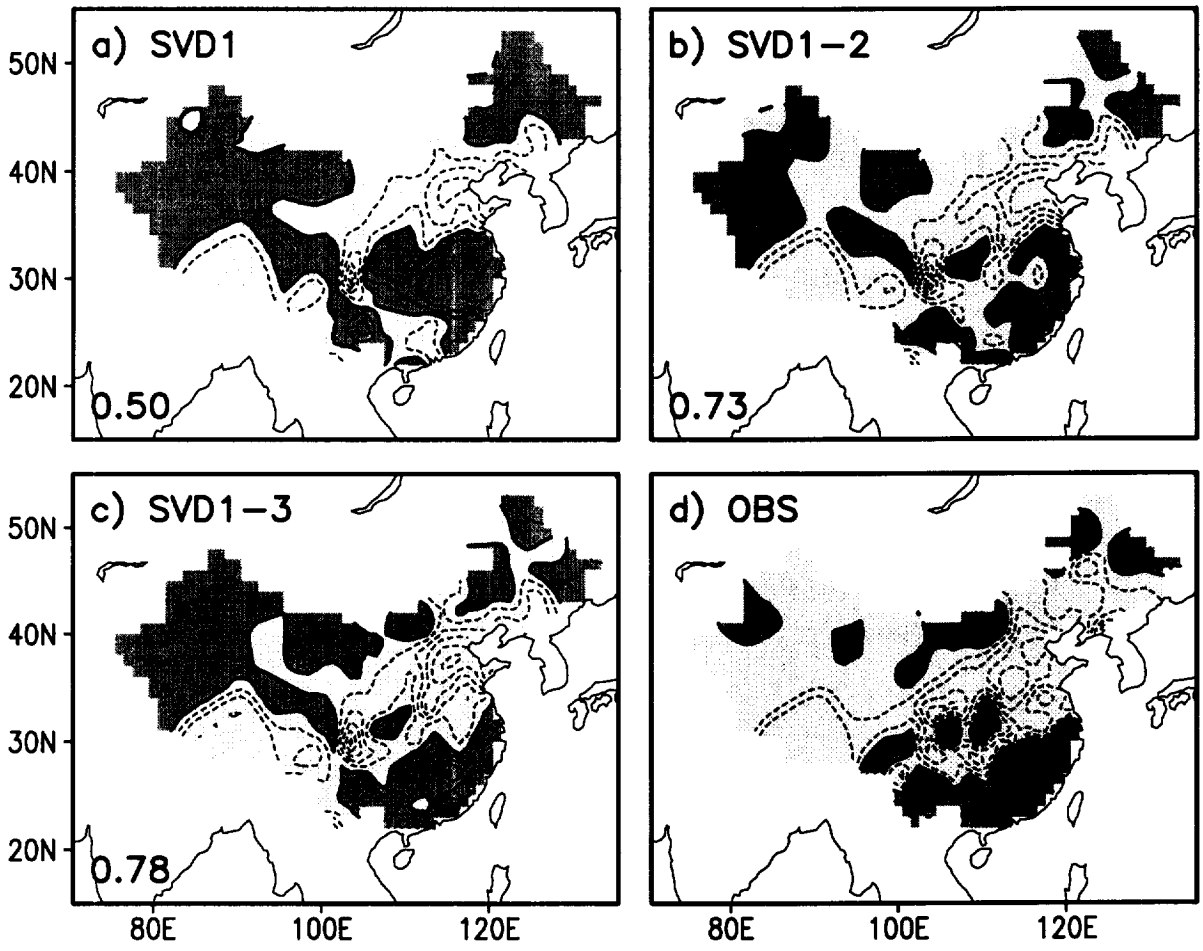
1997 JJA
a) SVD1
0.50
b) SVD1−2
0.73
c) SVD1−3
0.78
d) OBS
50N
40N
30N
20N
80E
100E
120E

Fig. 11

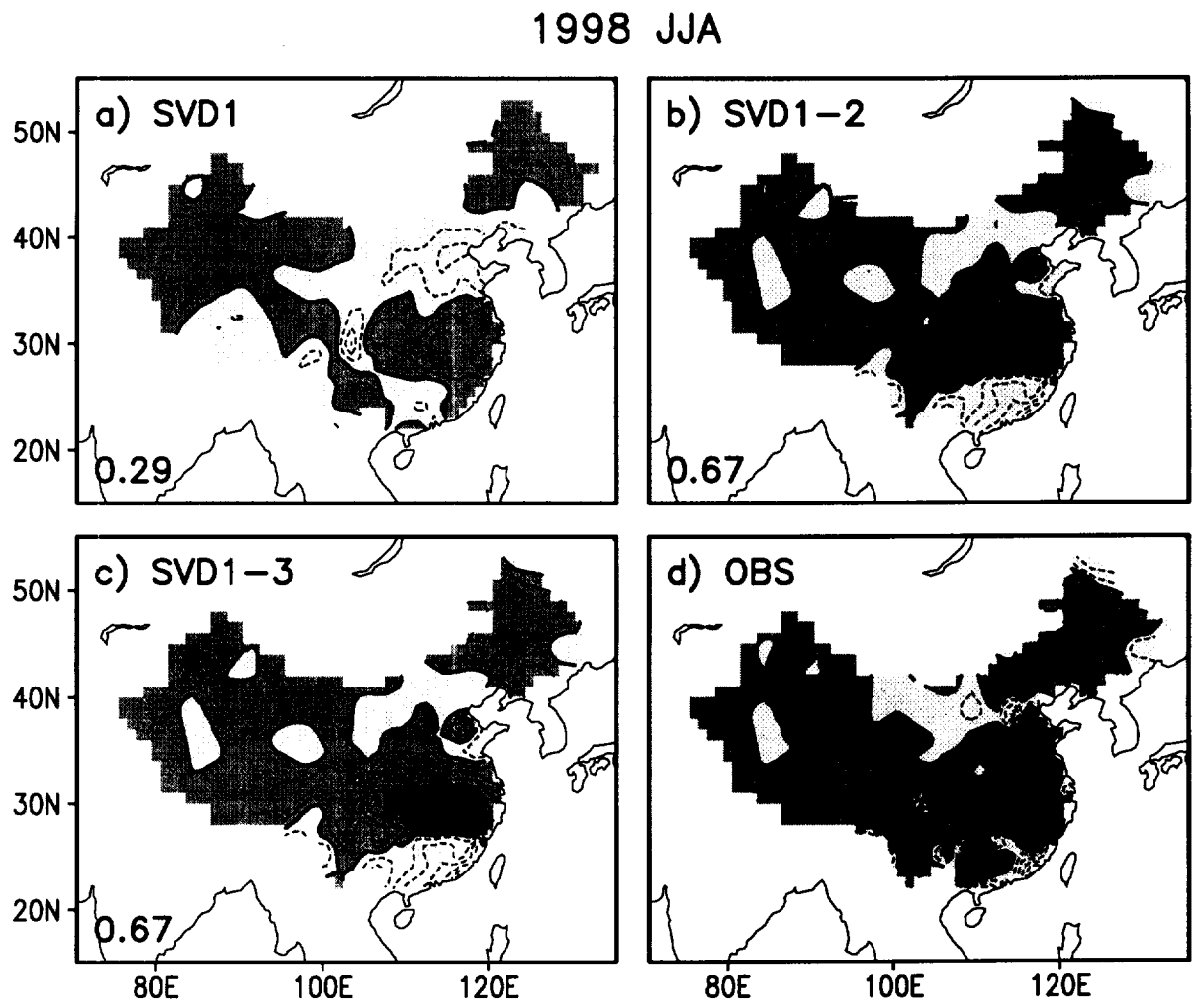
1998 JJA
a) SVD1
0.29
b) SVD1−2
0.67
c) SVD1−3
0.67
d) OBS
50N
40N
30N
20N
80E
100E
120E

Fig. 12

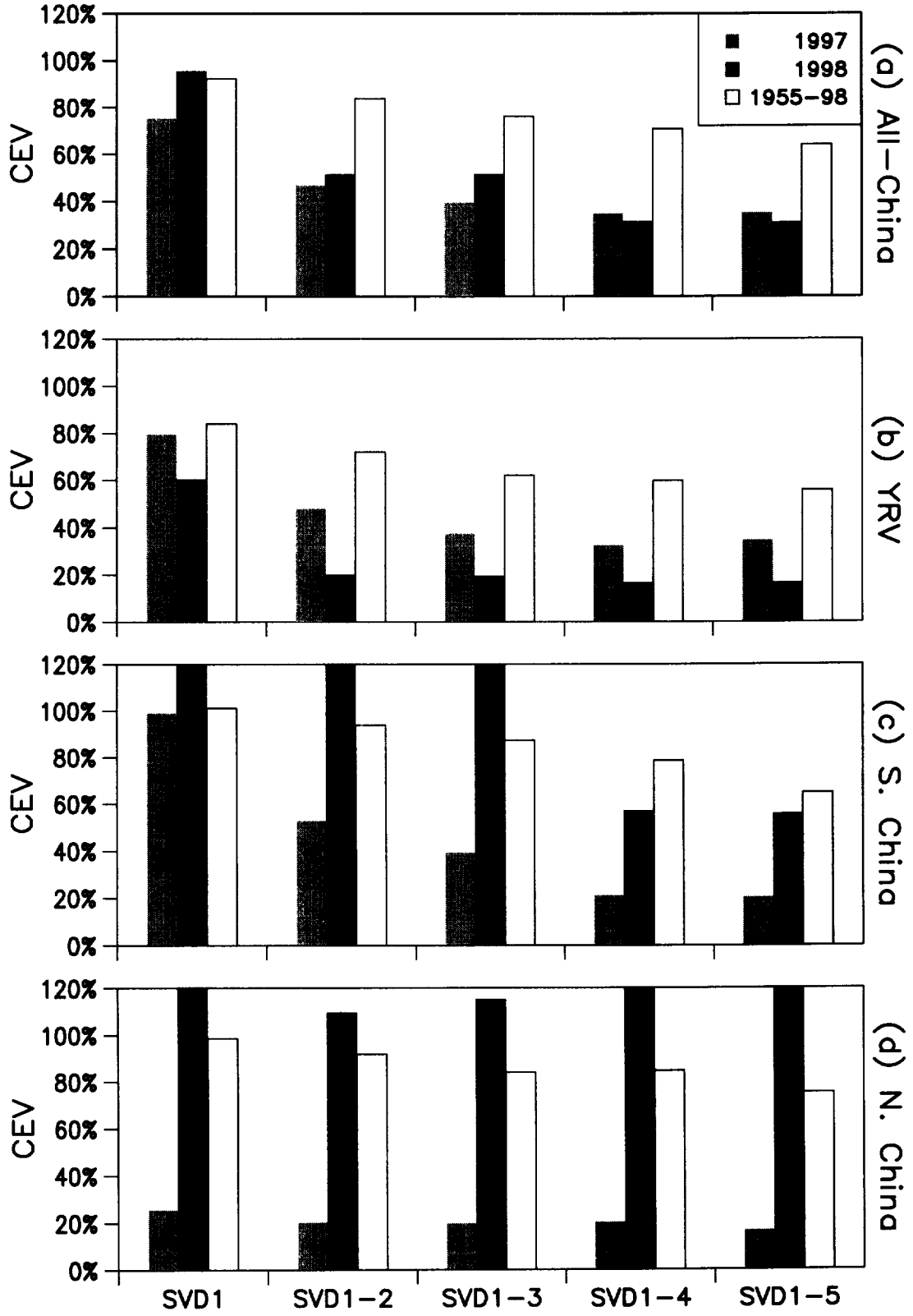
120%
100%
80%
60%
40%
20%
0%
CEV
1997
1998
1955-98
(a) All-China
(b) YRV
(c) S. China
(d) N. China
SVD1
SVD1-2
SVD1-3
SVD1-4
SVD1-5

Fig. 13